https://doi.org/10.1016/j.sna.2020.112007

An optimized Graphene/4H-SiC/Graphene MSM UV-photodetector operating in a wide range of temperature

H. Bencherif [1*], L. Dehimi[1,2], G. Messina[3], P. Vincent[4], F. Pezzimenti[3], F. G. Della Corte[3]

1.-Laboratory of Metallic and Semiconductor Materials, University of Biskra, Biskra, Algeria.
2.-Faculty of Science, University of Batna 1, Algeria
3.-DIIES, Mediterranea University of Reggio Calabria, Reggio Calabria, Italy.
4.-School of Electronics Engineering, Kyungpook National University, 80 Daehakro, Buk-gu, Daegu, 702-701, Republic of Korea.

* E-mail: hichem.bencherif@univ-batna2.dz, hichem.bencherifeln@gmail.com

Abstract

In this paper, .an accurate analytical model has been developed to optimize the performance of Interdigitated Graphene Electrode/p-silicon carbide (IGE/p-4H-SiC) Metal semiconductor Metal (MSM) photodetector operating in a wide range of temperatures. The proposed model considers different carrier loss mechanisms and can reproduce the experimental results well. An overall assessment of the electrodes geometrical parameters' influence on the device sensitivity and speed performances was executed. Our results confirm the excellent ability of the suggested Graphene electrodes system for decreasing the unwanted shadowing effect. A responsivity of *238 μA/W* was obtained under *325-nm* illumination compared to the *16.7 μA/W* for the conventional *Cr-Pd/p-SiC PD*. A photocurrent to- dark-current ratio (*PDCR)* of 5.75 × 10^5 at 300K and 270 at 500K was distinguished. The response time was found to be around 14 μs at 300K and 54.5 μs at 500K. Furthermore, the developed model serves as a fitness function for the multi objective optimization (MOGA) approach. The optimized *IGE/p-4H-SiC MSM-PD* design not only exhibits higher performance in terms of *PDCR* (7.2×10^5), responsivity ($430 A/cm^2$) and detectivity (1.3×10^{14} Jones) but also balances the compromise between ultrasensitive and high-speed figures of merit with a response time of 4.7 μs. Therefore, the proposed methodology permits to realize ultra-sensitive, high-speed SiC optoelectronic devices for extremely high temperature applications.

Keywords: UV photodetector, Analytical Model, Graphene, 4H-SiC, interdigitated electrodes, MOGA approach.

https://doi.org/10.1016/j.sna.2020.112007

1. Introduction

The incredible properties of Graphene based 2D material have been flooding scientific news for many years. Due to its outstanding performances such as high electrical conductivity, excellent optical transparency and mechanical flexibility, this material is well placed to pave the way to high-performance devices [1]. The amazing versatility of Graphene gave rise to multiple applications [2]. Recently, Graphene has been considered as a potential nominee for optoelectronic and photovoltaic applications. Usually, the photo-generated carriers collection mechanism in optoelectronic and photovoltaic devices is established using classical transparent conductors as Ni/Au, Ti, Cr/Pd and ITO [3–4]. Nevertheless, these materials show a reduced optical transmittance (< 80%) due to the elevated reflection at the surface which produces a dilemma for their utilization in optical fiber communication systems and optical speed interconnections [5]. In contrast to the aforementioned materials, zero band gap Graphene with a high transmittance exceeding 80% in the UV ultraviolet regime, is a potential alternative for transparent conductive electrode for future ultraviolet photodetectors (UV PDs) and solar cells [6-8]. Analogous to the aforesaid materials, a Schottky barrier can also be formed at the interface monolayer Graphene/SiC substrate [7]. The work function of Single layer Graphene is around $\emptyset_G$= 4.5 eV on 4H-SiC with an electron affinity of χ_{SiC} = 3.24 eV [9-11]. Newly, chemical vapor deposition (CVD) technique has been used to realize a monolayer Graphene transparent electrode for GaN Metal semiconductor Metal photodetector (MSM) UV PD [9]. Unlike GaN material the realization of such an electrode could be done readily on a SiC substrate using just vacuum annealing process at high temperature and therefore avoiding any deposition and/or transfer technique [10–11]. MSM UV PD made of silicon carbide, a wide band gap semiconductor (Eg = 3.24 eV at room temperature) that shows outstanding optical and physical properties in terms of high thermal conductivity, mechanical strength, and radiation hardness, has achieved a reputation for operating under harsh environments [12]. Low

cost and simple production process are the main features of a p-type silicon carbide in view of its use in optoelectronic applications. However, a high recombination of the photo-generated carriers affects the devices performances. Therefore, analytical or numerical models that quantify this degradation in photodetector based p-type SiC are of interest. Even at high temperatures the SiC based photodetector exhibited high responsivity and decreased leakage current [13]. Nevertheless, the SiC MSM-PD displayed an important drawback in terms of responsivity under the UV regime. In particular, the response time of tens of seconds is considered too long, and hinders the use of SiC MSM PD in ultrahigh response application. Therefore, numerous works have proposed the interdigitated electrode engineering as efficient strategy to minimize the PD time response throw downscaling the electrodes finger gap [14–16]. Otherwise the shadowing effects with reduced active area would cause a considerable degradation problem [15–17]. This scope of blurred vision, resulting from lack of information regarding both responsivity and response time trade-off, imposes a dilemma in optimizing the device capability. However, solving this dilemma with an efficient experimental investigation; would be costly and time consuming. Consequently, the development of an accurate analytical model is indispensable.

Herein, a monolayer Graphene's transmittance was obtained via the calculation of optical conductivity. Using the thermionic emission charge transport equation and considering the current loss mechanisms, i.e.; Auger, Shockley–Read–Hall, surface and radiative recombinations, an analytical optoelectronic model was developed to boost up the Interdigitated Graphene Electrode/p-silicon carbide (*IGE/4H-SiC) MSM UV-PD*. Furthermore, an extensive comparison of the proposed device was carried out by comparing it with the conventional Cr/Pd/4H-SiC MSM PD, where the proposed device outperforms the conventional device for a wide range of design parameters and temperatures. The proposed model serves as a fitness function to recognize the IGE formalism pattern which permits the enhancement of the

https://doi.org/10.1016/j.sna.2020.112007

performance of the proposed Gr/4H-SiC IE MSM PD using MOGA-based technique. The achieved results indicate that the suggested design methodology not only permits to realize a superior compromise amid responsivity and response time, but also shed light on the proposed device's ruggedness under high temperature conditions. This opens the way to realize ultra-sensitive, high-speed SiC optoelectronic devices for extremely high temperature applications.

2. UV photodetector structure

The proposed PD assessed in this work is depicted in Figure 1. From top to bottom, it consists of two adjacent Graphene electrode deposited on the p type 4H-SiC material. An isolation/passivation SiO_2 layer is inserted on the outside of Graphene finger electrodes.

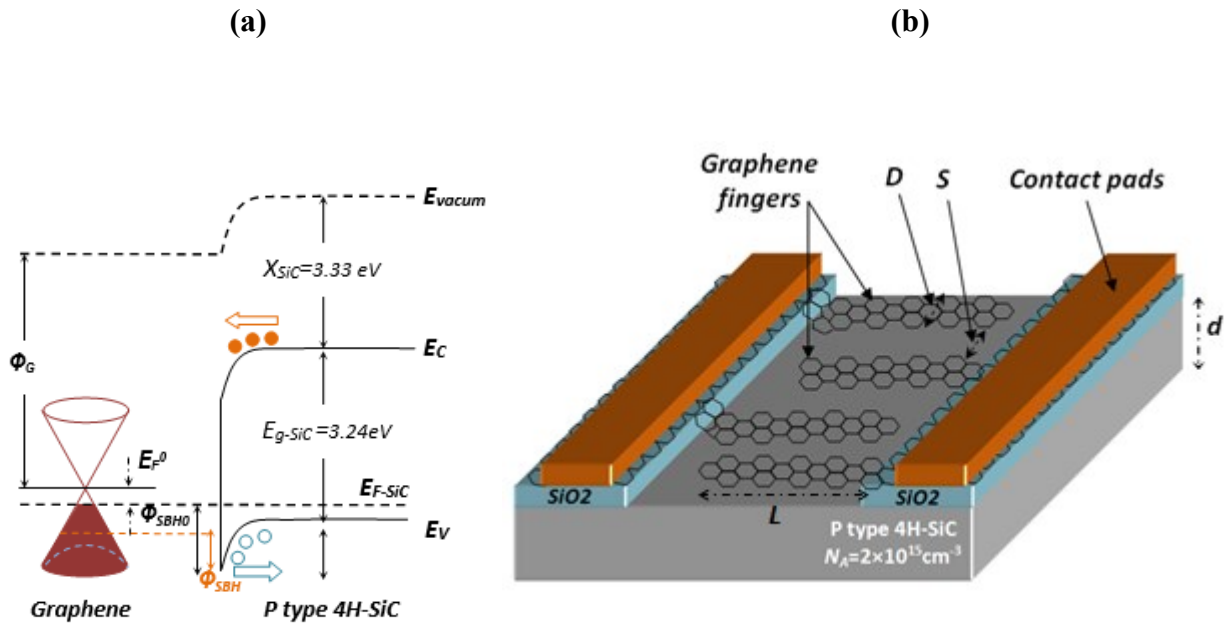

Figure 1. a) Energy band diagram of *Graphene/p-SiC/Graphene structure,* b) Cross-sectional view of the suggested *IGE/4H-SiC MSM UV-PD* with interdigitated electrodes.

In Fig.1-b, the parameters *S* and *D* refer to the gap between the fingers, and the width of the fingers of the *IGE/4H-SiC/IGE MSM-PD* interdigitated contact system, respectively. The parameter *L* denotes the receiving aperture and *d* refers to the p type 4H-SiC thickness. Low doped p type 4H-SiC permits the extension of the depletion region leading to a high electric

field at the IGE/p-SiC interfaces. This latter can enhance electron/hole pair's separation mechanisms and thus circumvents the recombination losses.

3. An analytical model

Herein, we propose a new analytical model that takes into consideration the carrier recombination effect. Besides, the incorporated improved Graphene transmission model that mimics the experimental results, the developed model provides a useful description of the effect of several geometric and electrical parameters on the proposed *IGE/4H-SiC MSM UV-PD* photodetector under high temperature condition.

3.1. Modeling of the photocurrent

The thermionic emission theory describes the current-voltage characteristic (*I-V*) by means of the following expression [18, 19]:

$$I = I_0 \exp\left(\frac{q(V - R_S I)}{nK_B T} - 1\right) + I_L \qquad (1)$$

where V represents the bias voltage, q represents the electron charge, n is the ideality factor, R_S is the series resistance, K_B is the Boltzmann constant, T is the temperature, and I_0 refers to the saturation current density, given by [20]:

$$I_0 = A^* S T^2 \exp\left(\frac{-q\varphi_{SBH}}{KT}\right) \qquad (2)$$

where S denotes the contact Graphene area, A^* is the effective Richardson constant, φ_{SBH} denotes the Schottky barrier height linked to the Graphene/SiC contact [21].

The light-generated current density I_L accounting for different recombination loss mechanisms is given as follows:

$$I_L = I_{ph} - I_{SRH} - I_{Aug} - I_{surf} - I_{rad} \qquad (5)$$

where I_{ph} represents the photo-generated carriers current density given by [18]:

https://doi.org/10.1016/j.sna.2020.112007

$$I_{ph} = -q\int_{0}^{W_D} G_e(x)dx = q\varphi_0\left[1-\exp(-\alpha W_D)\right] \quad (6)$$

where W_D refers to the depletion region width and φ_0 is the incident photon flux (in units of cm-2s-1) $G_e\ (x)$ (in units of $cm^{-3}\ s^{-1}$), denotes the generation rate defined by:

$$G_e(x) = \phi_0 \alpha \exp(-\alpha x) \quad (7)$$

where α is the absorption coefficient, which can be approximated using the following expression [22, 23]:

$$\alpha(T) = A\left[\frac{(h\nu - E_g(T) - E_{ph})^2}{1-\exp(-E_{ph}/KT)} + \frac{(h\nu - E_g(T) + E_{ph})^2}{\exp(+E_{ph}/KT)-1}\right] \quad (8)$$

where A and Eph denote, respectively, the absorption strength and phonon energy. Using the Passler formula, the band gap temperature dependence $E_g\ (T)$ can be expressed as follows [24]:

$$E_{gp}(T) = E_g(0) - \left(\varepsilon\zeta_p/2\right)\left(\sqrt[p]{1+(2T/\zeta_p)^p}-1\right) \quad (9)$$

here $\varepsilon = 3\times10^{-4}$ eVK^{-1}, $\zeta_p = 450K$ and p = 2.9

This expression is experimentally confirmed for all SiC polytypes for a wide range of temperature (77 - 500 K). In equation (6) φ_0 refers to the number of the incoming photons per unit area given by the following:

$$\phi_0 = \frac{P_{opt}\left(1-R_G\right)}{Ah\nu} \quad (10)$$

where A represent the device area in eq.8 and R_G denotes the graphene reflectivity, expressed as [25,26]

$$R_G(\omega) = \frac{\left|\sqrt{\varepsilon_1\varepsilon_{SiC}}\varepsilon_0 + \sqrt{\varepsilon_1}\sigma(\omega)/c - \varepsilon_1\varepsilon_0\right|^2}{\left|\sqrt{\varepsilon_1\varepsilon_{SiC}}\varepsilon_0 + \sqrt{\varepsilon_1}\sigma(\omega)/c + \varepsilon_1\varepsilon_0\right|^2} \quad (11)$$

https://doi.org/10.1016/j.sna.2020.112007

where ε_1 and ε_{SiC} represent, respectively, the dielectric constant of air and 4H-SiC, $\sigma(\omega)$ refers to the graphene optical conductivity expressed as follows: [27, 28].

$$\sigma(\omega)=\frac{2iq^2T}{\pi\hbar(\omega+(i/\tau))}\ln\left[2\cosh(\mu/2T)\right]+\frac{q^2}{4\hbar}\left[G(\omega/2)-\frac{4\omega}{i\pi}\int_0^{+\infty}dE\,\frac{G(E)-G(\omega/2)}{\omega^2-4E^2}\right] \quad (12)$$

where the first term in equation (12) refers to the electron– photon intraband scattering mechanism, where τ, $\hbar$ and μ denote the electron-disorder scattering processes, the reduced Plank constant and the chemical potential, respectively. The second term is linked to the direct inter band electron transitions. G refers to the Fermi levels difference calculated from G(E)= f_0(-E)- f_0(E), and it can be approximated as follows for numerical computations:

$$G(E)=\left(\frac{\sinh(E/T)}{\cosh(\mu/T)+\cosh(E/T)}\right) \quad (13)$$

The photocurrent considering the interdigitated contact system can be expressed as follows [17]

$$I_{ph}=q\varphi_0\left(\frac{S}{S+D}\right)\left[1-\exp\left(-\alpha W_D\right)\right] \quad (14)$$

where S and D represent, respectively the fingers gap and the finger's width of the investigated *IGE/4H-SiC MSM UV-PD*.

I_{SRH} represents the current owing to Shockley–Read–Hall recombination phenomenon linked to the presence of defects within the 4H-SiC active area, these defects act as the main carrier-lifetime killer in 4H–SiC and given by [29]

$$I_{SRH}(V)=\frac{qW_D}{2}S_c v_{th}N_t n_i e^{qV/2KT} \quad (15)$$

where n_i is the intrinsic carrier density, S_c and v_{th} denote, respectively, the capture cross section and the thermal velocity, N_t refers to the density of traps.

I_{Aug} represents the current due to Auger recombination occurrence, expressed as follows [30]

https://doi.org/10.1016/j.sna.2020.112007

$$I_{Aug} = q\int_{vol} R_{Aug} dv \qquad (16)$$

where R_{Aug} refers to the Auger recombination rate estimated from the following expression [18]:

$$R_{Auger} = \left(C_n n + C_p p\right)\left(pn - n_i^2\right) \quad (17)$$

where $C_{n(p)}$ represents the electrons (holes) Auger coefficient presented in table 1.

I_{surf} represents the current due to the surface recombination phenomenon, caused by traps located at the interface Graphene/semiconductor interface given by [31]:

$$R_{surf} = \frac{np - n_i^2}{S_n^{-1}(p + n_i) + S_p^{-1}(n + n_i)} \qquad (18)$$

where $S_{n(p)}$ denotes the electrons (holes) surface recombination velocity.

I_{rad} represents the radiative recombination current. The net recombination rate can be estimated using the following expression [18]:

$$R_{rad} = B\left(pn - n_i^2\right) \qquad (19)$$

where B refers to the radiative recombination coefficient expressed as follows [32]

$$B = \frac{1}{\pi^2 \hbar^3 c^2 n_i^2}\int_0^\infty n_r^2 (\hbar\omega)^2 \alpha(\omega) \exp\left(\frac{-\hbar\omega}{KT}\right) d(\hbar\omega) \qquad (20)$$

where c and n_r denote the light speed and the 4H-SiC refractive index, with this latter listed in Table 1.

Table.1. 4H-SiC physical parameters

Parameters of 4H-SiC	**Value**	**References**
Affinity	3.33 eV	[34]
Thermal Conductivity, λ (W/cmK)	4.5	[35]
Refractive index, n_r	2.4	[35]
Auger coefficient, $cm^6\ s^{-1}$	$7\pm1\times10^{-31}$	[36]
Surface recombination velocity ($cm\ s^{-1}$)	10^4	[37]
Carrier saturation velocity, v_{sat} (cm/s)	2×10^7	[38]

https://doi.org/10.1016/j.sna.2020.112007

To finish, the Caughey–Thomas temperature-dependent carrier mobility model confirmed for SiC material is considered [33].

3.2. Modeling of the response time

The main response time of the proposed *IGE/4H-SiC MSM UV-PD* can be calculated by combining the contribution of both the transit and RC times as follows [16,17]:

$$\tau = \quad (\tau^2{}_{dr} + \tau^2{}_{RC})^{\frac{1}{2}} \qquad (21)$$

The transit time for the fully depleted active region is given by [17]:

$$\tau_{dr} = \frac{D\chi}{2V} \qquad (22)$$

$$\frac{1}{V^4} = \frac{1}{2}\left(\frac{1}{V_e^4} + \frac{1}{V_h^4}\right) \qquad (22\text{-a})$$

where χ and V denote ,the corrective coefficient of the carrier drift distance and carrier drift mean velocity, respectively. V_e and V_h denote the saturation velocities of both electrons and holes.

The second term of eq (21) refers to the RC-time of the interdigitated design defined by [39]:

$$\tau_{RC} = 2.2RC \qquad (23)$$

By using a conformal mapping based approach the capacitance of the engineered interdigitated structure can be calculated as follows [40]:

$$C = 0.226NL\varepsilon_0(\varepsilon_s + 1)\frac{K(\sin\eta\frac{\pi}{2})}{K(\cos\eta\frac{\pi}{2})} \qquad (24)$$

where ε_0 and ε_s represent the vacuum permittivity and the semiconductor relative permittivity, respectively. N denotes the finger pairs number calculated from $N=L/2(S+D)$, η is the finger period ratio expressed as $\eta=D/(S+D)$. In equation (24) the coefficient K can be calculated by [16]:

https://doi.org/10.1016/j.sna.2020.112007

$$K = \int_0^{\pi/2} \frac{dx}{\sqrt{1-k^2\sin^2 x}}, \quad k = \sin\eta\frac{\pi}{2} \quad (25)$$

The effect of interdigitated electrodes formalism on the investigated Gr/SiC/Gr performances *PDCR* and responsivity can be examined via the following expression [18, 26]:

$$PDCR = \frac{I_{ph} - I_D}{I_D} \quad (26)$$

$$R = \frac{I_{ph}(A)}{P_{inc}(W)} \quad (27)$$

where *PDCR* and *R* denote the photocurrent to dark current ratio and the responsivity, respectively, P_{inc} represents the incident power.

4. Results and discussions

4.1. Model validation

For the purpose of testing the accuracy of the developed model, the *I-V* characteristics of the conventional Cr-Pd/4H-SiC MSM PD is compared with experimental data [41]. From figure 2 a close agreement was noticed which validates the accuracy of the assumed model. The slight difference observed was mainly due to the 4H-SiC series resistance and the accumulated charges at the interface related to the Schottky barrier lowering. The obtained outputs of both analytical model and experimental structures are summarized in table 2.

https://doi.org/10.1016/j.sna.2020.112007

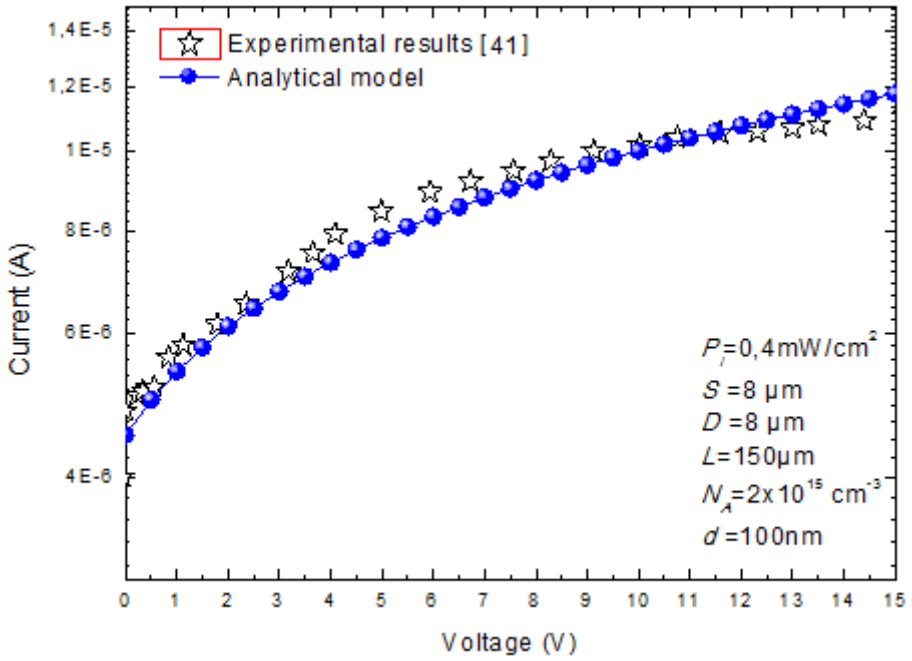

Figure 2. *I–V* curves of the conventional 4H–SiC MSM PDs measured and analytical model under illumination at room temperature (P_i = 0.4 mW/cm^2, λ=325nm, S=8µm, D=8µm, L=150µm, d=100 nm, N_a= 2×10^{15}cm^{-3}).

Table 2. Electrical output comparison between the experimental results and the analytical model at room temperature at 5V

Parameters	***Responsivity (mA/W)***	***PDCR***	I_{dark} ***(A)***
Experimental results [41]	16.7	1.3×10^5	6×10^{-11}
Analytical model	16.58	1.15×10^5	6.4×10^{-11}

It is of interest to investigate the influence of the established IGE system on the device sensitivity and speed figures of merit. Figure 3 shows the variation of both dark and photocurrent densities of the proposed and conventional devices as a function of biasing voltage. The simulations were performed under UV light with 325 nm and an incident optical power of 0.4 mW/cm^2.

https://doi.org/10.1016/j.sna.2020.112007

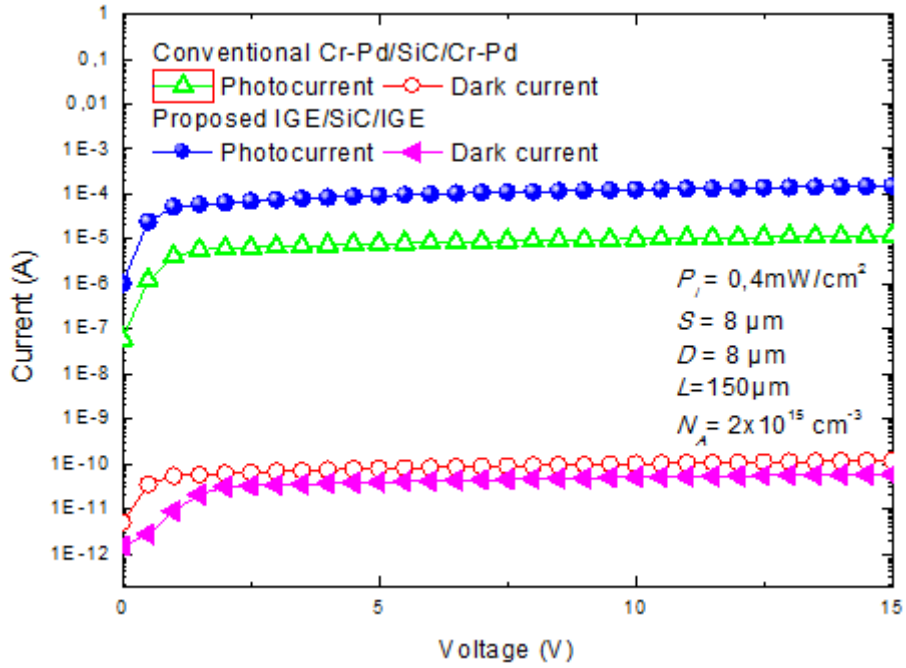

Figure 3 *I–V* curves of the proposed *IGE/4H-SiC MSM UV-PD* and the conventional device (P_i = 0.4 mW/cm^2, λ=325nm, *S*=8µm, *D*=8µm, *L*=150µm, *d*=100nm, N_a= 2×10^{15}cm^{-3},*V*= 5 V).

As illustrated in figure 3, the suggested *IGE/4H-SiC* structure reveals a better derived current with respect to the conventional *Cr-Pd/4H-SiC MSM PD*. This fact is due principally to the high transparency of Graphene electrodes, which decreases the unwanted shadowing effect and thus boosts surprisingly the optical absorption in the device active area. Besides, the high carrier mobility ensured by Graphene sheet permits efficient photo-generated carriers collection mechanism which enhances the efficacy of carrier transport. A further finding that adds an outstanding feature to the proposed *IGE/4H-SiC MSM UV-PD* is the lower dark current, which can enhance efficiently the *PDCR* in contrast to the conventional device. This feature is due to the improved Schottky barrier height using Graphene electrodes. This means, that an increased Schottky barrier, causes an improved interfacial electric field and thus the built-in voltage conducts to strong rectification and an increased dissociation rate of bound electron–hole pairs and photo-generated current. Since, the electrodes had a direct influence on the PD performances, it seems beneficial to investigate systematically the interdigitated system's geometrical parameters impact on the devices optical and electrical performances. Within this

https://doi.org/10.1016/j.sna.2020.112007

framework, Fig. 4 (a) depicts the responsivity and the I_{ON}/I_{OFF} ratio versus the fingers gap. It is interesting to note that a downscale of the finger gap causes a high shadowing effect in the sensing active area, which leads to decreased device performances.

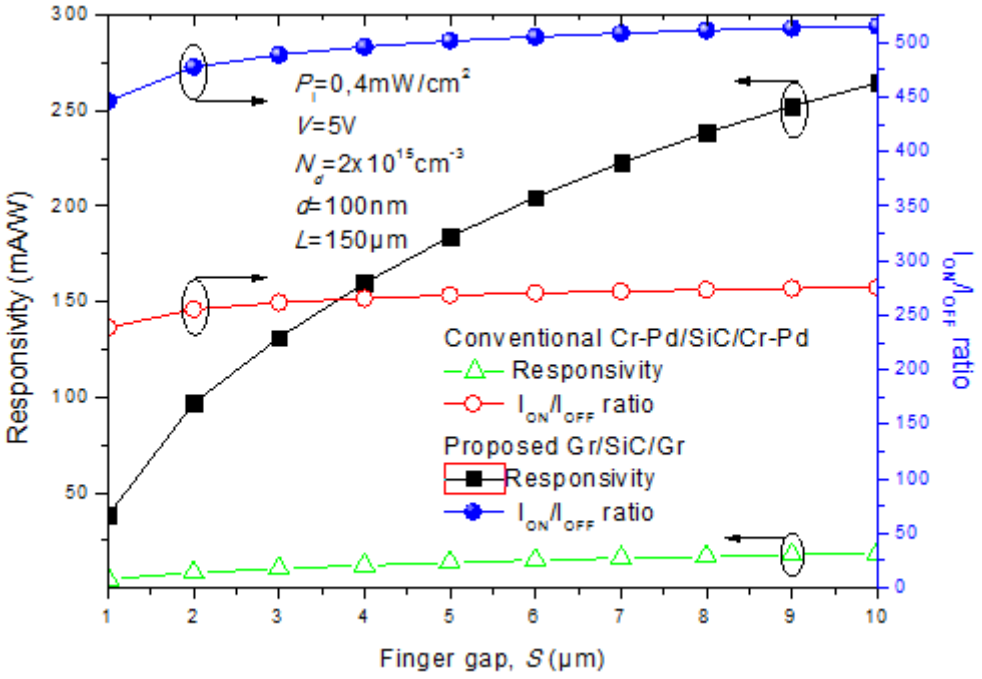

(a)

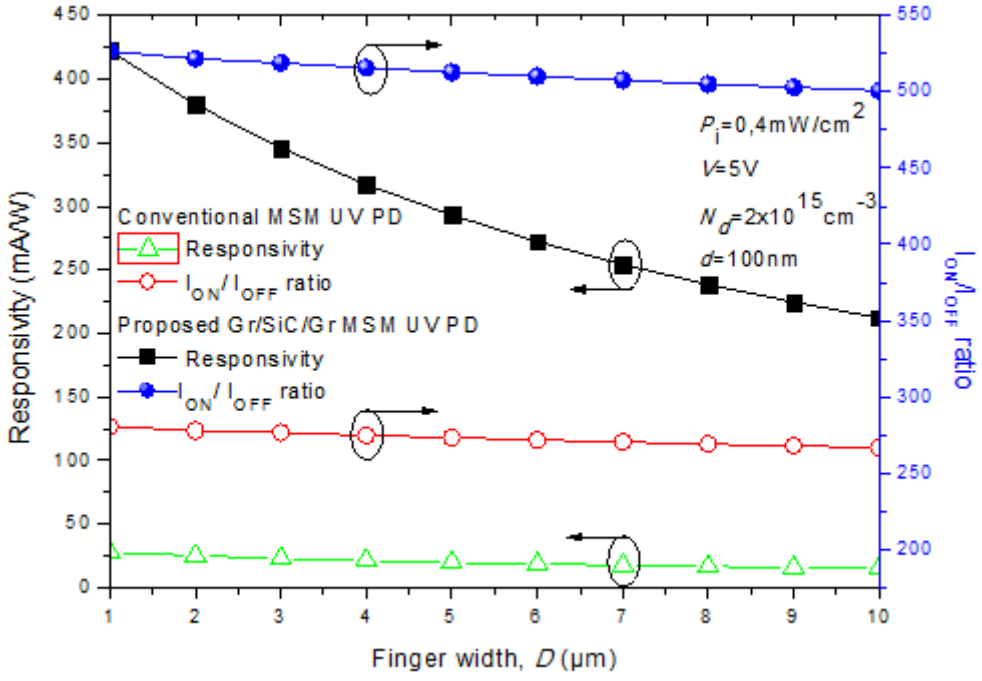

(b)

https://doi.org/10.1016/j.sna.2020.112007

Figure 4. The responsivity and I_{ON}/I_{OFF} ratio versus (a) electrodes gap (b) electrode width for both proposed *IGE/4H-SiC MSM UV-PD* and conventional Cr-Pd/SiC/Cr-Pd (P_i = 0.4 mW/cm^2, λ=325nm, L=150µm, d=100nm, N_a= 2×10^{15}cm^{-3},V= 5 V).

From figure 4 the proposed *IGE/4H-SiC MSM UV-PD* reveals a high responsivity (238.5mA/W) under the unwanted shadowing effect than conventional design with Cr/Pd electrodes (4.8 mA/W). Besides, the proposed PD shows a high dependency on the fingers gap variation, where the more the gap increase the more the responsivity and the I_{ON}/I_{OFF} ratio are improved. This fact is due to the reduced *IGE/4H-SiC MSM UV-PD* structure reflection and the superior transparency offered by the Graphene sheet. The proposed PD displays a 90% enhancement in terms of both responsivity and I_{ON}/I_{OFF} ratio for a fingers gap of 1µm and a 50% and 20% for 10µm. Consequently, the suggested *IGE/4H-SiC MSM UV-PD* design gives promising opportunities for further improving the device optical capabilities.

In order to optimize the optical and electrical performances of the proposed PD, targeting the suppression of the degradation linked to the shadowing effect is required. In what follows, further investigations on the system design parameters are displayed. Figure 4 (b) shows the responsivity and the I_{ON}/I_{OFF} ratio variations versus electrodes width. It is obvious from this figure that the proposed PD design surpasses the conventional one, where a high responsivity (238.5mA/W) and superior I_{ON}/I_{OFF} ratio (505) are reached through the use of Graphene interdigitated electrodes which reveals a 53% improvement compared to the conventional *PD* using Cr/Pd electrodes for the same electrode width ($D=8\mu m$). In addition, a decrease in the device's capabilities is observed when increasing the electrodes width. This fact is mainly due to the expansion of the shaded area. The promising results can be attributed to the superior optical features of Graphene material (high transparency and less reflection of the incident light) which permit the reduction of the shaded area by controlling the electrodes width. As a result, several potential features are attained using the proposed Graphene electrodes system. The high transparency and low reflectivity provided by the Graphene material choice, assures a better

https://doi.org/10.1016/j.sna.2020.112007

absorption in the device sensing active area. In addition, the high mobility and the enhanced Schottky contact barrier provided by the Graphene electrodes serves in improving the device's charge transport ability. By combining the obtained results from figure (a) and (b), we can deduce that the proposed PD offers a way to further optimize the PD performances through controlling the geometry design unlike the conventional device, which remains not affected by the electrodes parameters variations. This can be linked to the high degradation caused by the electrode material shadowing effect.

It is a common knowledge that *PDCR* offers a straight insight about dark current and responsivity. As an objective assessment sensing capability, the photocurrent-to-dark-current ratio (*PDCR*), is given by [21]:

$$PDCR = (I_{ph}-I_d) / I_d \quad (28)$$

where I_{ph} and I_d represent the photocurrent and dark current, respectively, for an incident power P_i=0.4mW.

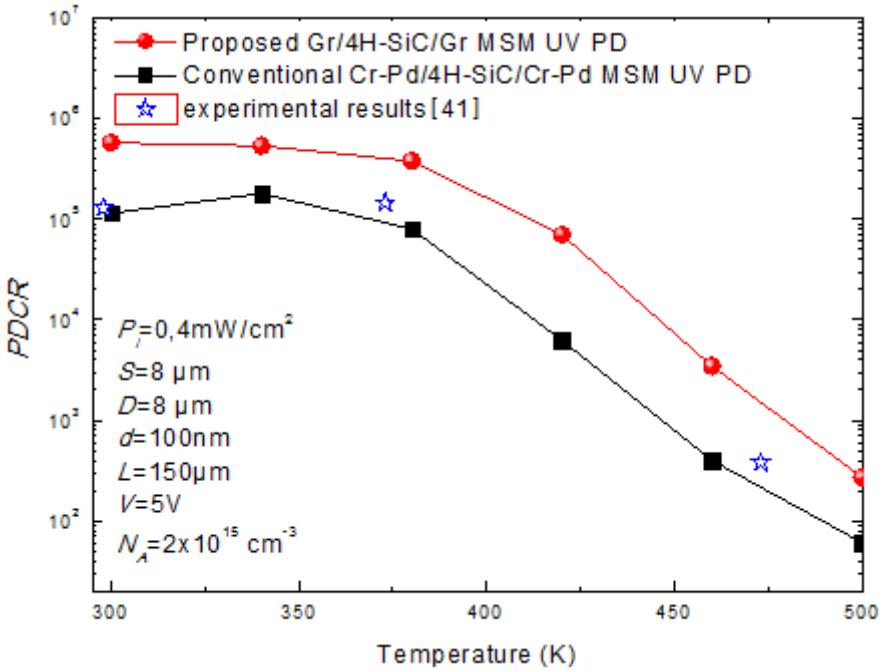

Figure 5. Variation of *PDCR* as a function of temperature (P_i = 0.4 mW/cm^2, λ=325nm, S=8µm, D=8µm, L=150µm, d=100nm, N_a= 2×10^{15}cm^{-3},V= 5 V).

https://doi.org/10.1016/j.sna.2020.112007

Figure 5 depicts the *PDCR* variation as function of temperature. It is observed that the photocurrent-to-dark-current ratio (*PDCR*) decreases as the temperature increase. This is mainly caused by the thermal carrier generation which elevates the dark current. Besides, the proposed *IGE/4H-SiC MSM UV-PD* shows a lower degradation when compared to the conventional device. This due to the resulting low dark current when using Graphene electrodes. It is worthy to notice that the proposed device's UV light sensing was considerable under high temperature with *PDCR* higher than the silicon counterpart *PD* [21]. This is related to the 4H–SiC film's high thermal stability and low dark currents. As stated in the introduction, our aim is to investigate effect of the the interdigitated electrodes parameters design on the device speed and sensing capability. Figure 6 depicts the transit time variation versus the finger's gap with sweeping the electrodes length (50, 75,100,125,150 µm).

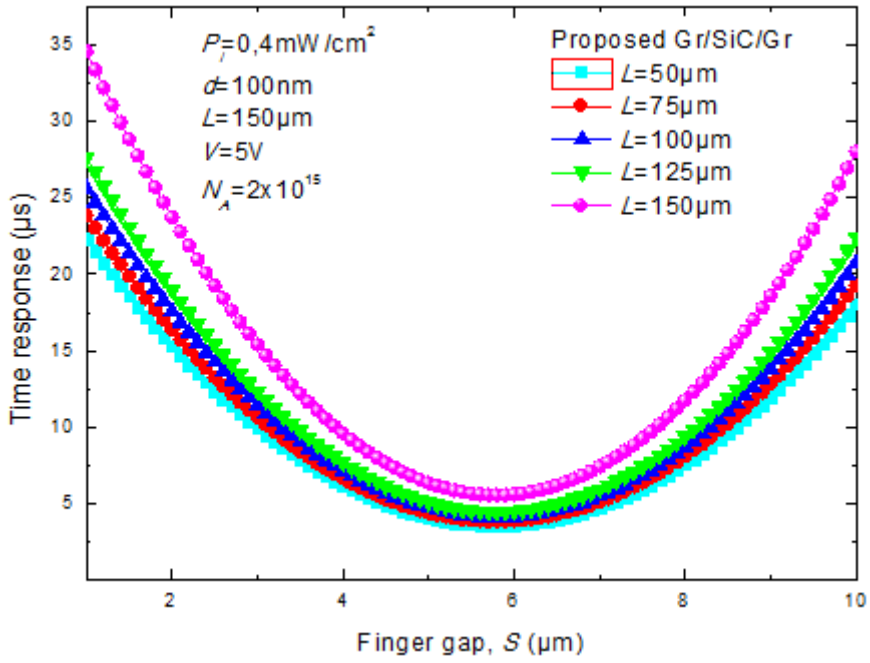

Figure 6. Time response versus finger gap for different electrodes length (L=50,75,700,125,150µm).

From figure 6 we can observe a decrease in the response time when reducing the finger's gap till value around 5.5 µm, then the time rises again. This complex behavior makes improving device speed more difficult when accounting for responsivity. Besides, by downscaling the

https://doi.org/10.1016/j.sna.2020.112007

finger's length the response time is decreased. In order to emphasize the proposed *PD* ruggedness at high temperature, the time response and the photocurrent as function of temperature are illustrated in figure.7.

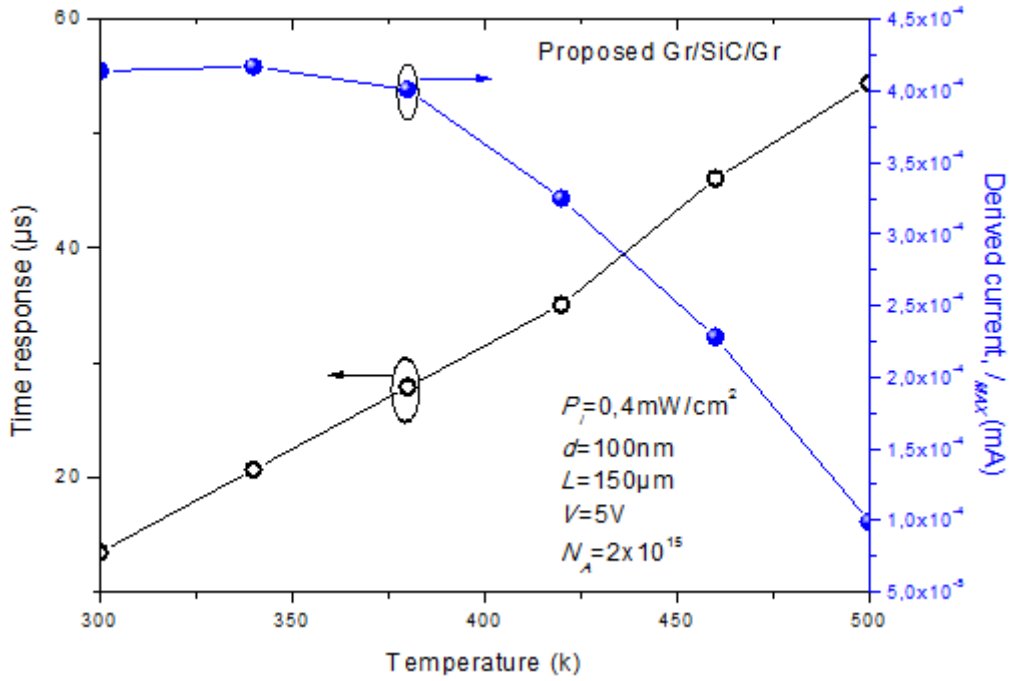

Figure 7. Time response and derived current as function of temperature (P_i = 0.4 mW/cm^2, λ=325nm, S=8µm, D=8µm, L=150µm, d=100nm, N_A= 2×10^{15}cm^{-3},V= 5 V).

As exposed in this figure the proposed device shows response time of (13.45µs) at room temperature, However, the more the temperature rises the more the degradation increase and a value of (54.5µs) is recorded for 500K, this is caused essentially by the proportional relationship related the transit-time-limited bandwidth and the saturation velocity for unchanging finger's gap [42].

$$f_{tr} = \left(0.441 \Big/ \sqrt{2}\right)(vs/s) \quad (31)$$

where f_{tr} represent the transit-time-limited 3-dB bandwidth, S and v_s denote ,respectively, the finger's gap and the saturation velocity. As the temperature increases the 4H–SiC hole/electron saturation velocity is minimized [43]. This reduces the bandwidth, and consequently, decreases

the *PD* speed under a high temperature condition. In addition, we observe from figure 7 that I_{ph} augments faintly with rising temperature (300-350). This due to the increase of the generated hole-electron pairs. However, at elevated temperature (350-500), I_{ph} diminishes. This is due to the increase in radiative recombination. Figure 7 confirms the ruggedness of the proposed *IGE/4H-SiC MSM UV-PD* under the harsh effect of temperature. The suggested UV sensor demonstrates a considerable current generation capability at elevated temperature level which is a handicap for the Si counterpart. This property makes our device appropriate for nanoscale applications under high temperature condition that need a fast time response and self-sufficient functionality.

4.2. Optimized *IGE/4H-SiC UV PD* design using MOGA optimization approach

The analysis established in the previous section on the influence of inherent physical and geometrical parameters on the performance of the considered *IGE/4H-SiC MSM UV-PD* reveals the interweaving effects of these parameters. Hence, an optimal solution that takes into account these facts must be found in order to get higher performances. The set of design parameters will constitute new criteria that permit to establish a multiobjective optimization. The denomination 'multiobjective' is linked to the fact that several objective functions have to be optimized simultaneously. Recently, A MOGA based method inspired by Darwin's evolution and natural selection theory has gained a great interest in the scientific community. They encompassed many areas and especially used for nonlinear optimization [44-48]. The background of the MOGA based optimization technique consists in establishing many arguments, such as objective functions, design constraints and parameters. Figure 8 depicts the flowchart of the suggested method used to optimize the speed and optical performances of the proposed *4H-SiC MSM UV-PD*. By bio mimicry considerations, each combination of design parameters X (S, D, L, d, N, Φ_G , N_A) is binary coded and called a chromosome. The constraints define the excursion of the variables allowed by the designer with respect to physical considerations. The crossover

https://doi.org/10.1016/j.sna.2020.112007

and mutation of several chromosomes from a set of population yield to a new chromosome. Then, the step of comparison is performed with selection operator and it favors the best that remain for the next evolution. For our optimization investigation based on MOGA, selection tournament and crossover operators are used in our GA to create a random vector.

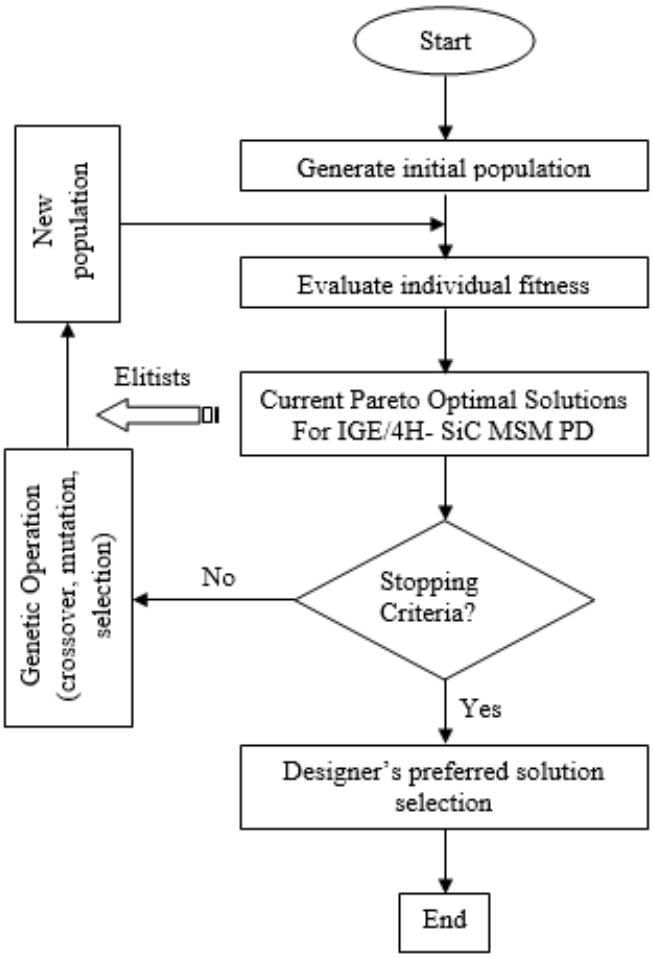

Figure 8. Schematic flowchart for a multi-objective genetic algorithm

The proposed methodology combines both Graphene electrodes formalism and evolutionary algorithm to offer multitude solutions to the designers, ie; High responsivity for environmental applications, high response time for optical communication systems, or a compromise for other applications.

https://doi.org/10.1016/j.sna.2020.112007

In the case of *IGE/4H-SiC MSM UV-PD*, three objective functions are needed; and their concern Responsivity, *PDCR* and time response. The optimization of the considered device is established according to the following goals:

– Maximization of the Responsivity, *Responsivity (X),*

– Maximization of the photocurrent to dark current ratio, *PDCR (X),*

– Minimization of the Time response (X), $\tau(X)$.

Where $X=\{S, D, L, d, N, \Phi_G, N_A\}$ represents the design variables vector. The constraints define the excursion of the variables allowed by the designer with respect to physical considerations. For the present investigation, they are expressed by:

– $g_1(x)$ where $x \in X$ is defined according to its own excursion, i.e., $x_{\min} \le x \le x_{\max}$.

– $g_2(x) : S \ge D$.

For our optimization investigation based on MOGA, scattered crossover techniques and tournament selection are used in our MOGA to produce a random vector. In order to incorporate the three objective functions in a single function we use the weighted sum approach. In this case, the resulting objective function is expressed as:

$$F(X)=w_1\,(1/Responsivity)+ w_2\,(1/PDCR)+ w_3\,(\tau) \quad (30)$$

It is worthy noticed that the optimal solution varies according to the weighting factors values of the overall objective function. For our study $w\ (i = 1\text{-}3)$ can be assigned equal values as 1/3.

https://doi.org/10.1016/j.sna.2020.112007

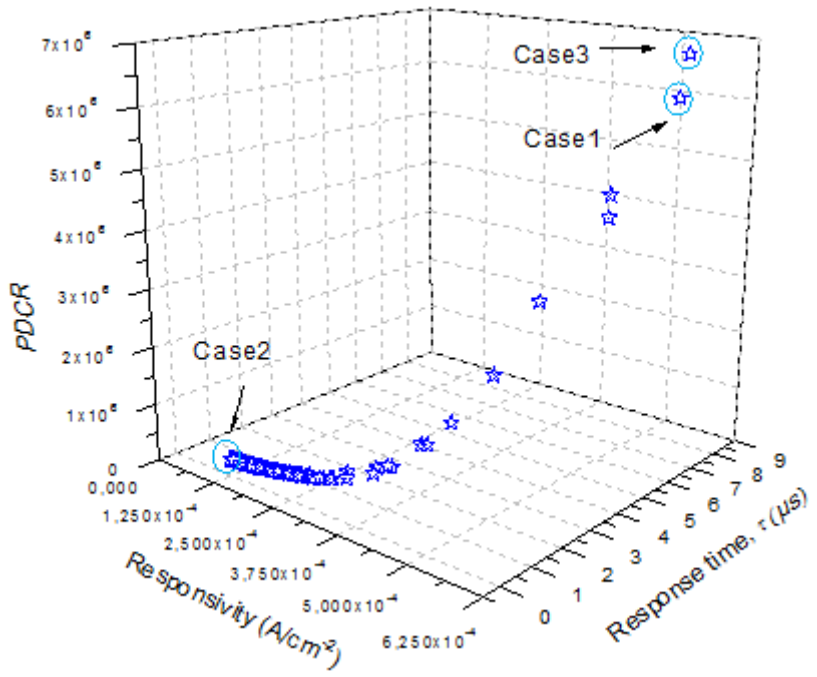

Figure 9. Pareto-optimal solutions of the proposed IGE/ SiC/IGE MSM UV PD.

A distinctive feature of the MOGA based optimization techniques is the flexibility in finding a set of solutions (Pareto front). Figure 9 depicts the Pareto front with the considered objective functions. Each of solution (*Responsivity* (x), *PDCR* (x) and $\tau(x)$) corresponds to the specific design variables. It can be clearly seen, that Pareto front offers the designer a multitude of choices according to his applications. In this case, three combinations are considered to assess the efficiency of the suggested optimization (see table 3).

Table 3 Optimized IGE/4H-SiC MSM UV-PD design parameters.

Design parameters	***Case 1***	***Case 2***	***Case 3***
Fingers design parameters			
electrodes gap *s(μm)*	10	5	10
electrodes width *D* (*μm*)	1.5	4	2.5
Finger's length *L(μm)*	115	50	125
Number of finger pairs *N*	5	3	5
MSM-PD design parameters:			
P–*SiC* doping concentration, $N_A(cm^{-3})$	2×10^{15}	1×10^{16}	5×10^{15}
P–SiC Film thickness, *d (nm)*	120	100	150
Objective functions			
Responsivity (*mA/W*)	420	100	410
Response time (*μs*)	7.52	1.65	8.1
PDCR (photo to dark current ratio)	5.9×10^{5}	8.3×10^{4}	6.75×10^{5}

https://doi.org/10.1016/j.sna.2020.112007

It is very beneficial to boost up the UV MSM PD namely speed and optical figure of merits, using the proposed methodology that combines Graphene interdigitated electrode formalism with MOGA metaheuristic approach. Within this framework, Table .4 compares the photodetector figure of merits of the optimized *IGE/4H-SiC MSM UV-PD* and the conventional structures.

Table 4. Comparison between optimized IGE/4H-SiC UV-PD and conventional structures.

Design parameters	**Au/TiO_2 MSM UV PD exp. results [49]**	**Pt/TiO_2 MSM UV PD [17]**	**Conventional Cr-Pd/SiC MSM UV PD exp. results [41]**	**Optimized IGE/4H-SiC MSM UV-PD**
Fingers design parameters				
electrodes gap *s(μm)*	25	10	8	9.7
electrodes Width *D* (*μm*)	35	10	8	1
Finger's length *L(μm)*	600	680	150	110
Number of finger pairs *Nf*	6	17	15	5
Metal work function (*eV*)	5.1 (Au)	6.1 (Pt)	4.5/5.6 (Cr/Pd)	4.5
MSM-PD design parameters:				
Wave length, λ(nm)	365	365	325	325
SiC doping concentration, $N_A(cm^{-3})$	/	/	P type 2×10^{15}	P type 2×10^{15}
P–SiC Film thickness, *d (nm)*	/	/	100	150
TiO_2 doping concentration (cm^{-3})	N type 2×10^{18}	/	/	/
TiO_2 thickness (nm)	200	200	/	/
Objective functions				
Responsivity (*mA/W*)	69.7	86.2	16.7	430
Detectivity (Jones)	/	8.5×10^{10}	3×10^{12}	1.3×10^{14}
Response time (*μs*)	1850	720	594	4. 7
PDCR (photo to dark current ratio)	0.74×10^{2}	2×10^{3}	1.3×10^{5}	7.2×10^{5}
LDR (linear dynamic range)	/	84.5	222.5	308.7

From table 4, it is clearly proved that the optimized Gr/SiC/Gr structure with Graphene electrode formalism display a better performances, where a high responsivity of (*430 mA/W)* is achieved when comparing to the conventional PD (*16.7 mA/W*) [41]. The optimized Gr/p-SiC/Gr MSM-UV-PD shows high sensitivity, and derived current ability than the conventional device. Moreover, the optimized Gr/SiC/Gr UV PD not only reveals an excellent ability for attaining a high *PDCR* value (7.2×10^5) than the conventional Cr-Pd based MSM-UV-PD (1.3×10^5), but also shows an improved specific detectivity value (1.3×10^{14} Jones) and large linear dynamic range (*LDR*) (308.7 dB). This finding proves the capability of our proposed method in overcoming the trade of low transit time (4.7 μs) and a high responsivity (430

mA/W). This lies in the decreased reflection losses and the suppression of the unwanted shadowing effects attained using the combined Graphene electrodes formalism and MOGA global optimization approach. The proposed design methodology serves efficiently to surmount the trade-off between responsivity and speed response. In brief, the suggested design methodology provides an easy way to recognize the suitable p-4H-SiC-MSM-UV-PD for a specific application.

Conclusion

In this work, an optimized *IGE/p-4H-SiC MSM UV PD* operating in a wide range of temperature has been analytically investigated, where an optoelectronic analytical model that considers different carrier loss mechanisms has been developed. In order to identify the appropriate parameters design we spotlighted the interweaving effects of different interdigitated system parameters on the device figure of merits. The results confirm the interdigitated Graphene formalism ability in improving the device performance, which allows the enhancement of the *IGE/p-4H-SiC MSM UV PD* reliability against the unwanted shadowing effect. In order to boost the device performance, a MOGA-based optimization approach has been successfully implemented in the context of our investigation, where the optimized design outperforms considerably the conventional designs.

https://doi.org/10.1016/j.sna.2020.112007

Acknowledgements

This work was supported by DGRSDT Of Ministry of Higher education of Algeria. The work was done in the unit of research of materials and renewable energies (URMER).

References

[1] C. Xie, Y. Wang, Z-X. Zhang, D. Wang, L-B. Luo, "Graphene/Semiconductor Hybrid Heterostructures for Optoelectronic Device Applications", Nano Today, vol.19, pp. 41-83, 2018. doi: 10.1016/j.nantod.2018.02.009

[2] Xinge Yu, Tobin J. Marks, and Antonio Facchetti, "Metal oxides for optoelectronic applications", Nature Materials, vol. 15, pp. 383-396, 2016. doi: 10.1038/NMAT4599.

[3] C K. Wang, S-J. Chang, Y-K. Su, Y-Z. Chiou, S C. Chen, C S. Chang, T K. Lin, H L. Liu and J J. Tang, "GaN MSM UV photodetectors with titanium tungsten transparent electrodes", IEEE Trans. Electron. Devices, vol.53, pp.38–42, 2006. doi: 10.1109/TED.2005.860780.

[4] F.G. Della Corte, F. Pezzimenti, R. Nipoti, "Simulation and experimental results on the forward J–V characteristic of Al implanted 4H–SiC p–i–n diodes", Microelectronics Journal, vol. 38, pp. 1273–1279, 2007. doi: 10.1016/j.mejo.2007.09.024.

[5] Z. Alaie, S. M. Nejad, M. H. Yousefi, "Recent advances in ultraviolet photodetectors", Materials Science in Semiconductor Processing, vol.29, pp.16-55, 2015. doi: 10.1016/j.mssp.2014.02.054.

[6] Z. Arefinia, A.Asgari, "Novel attributes in modeling and optimizing of the new graphene based $In_xGa_{1-x}N$ Schottky barrier solar cells", Journal of Applied Physics, vol.115(19), pp.194506, 2014. doi: 10.1063/1.4878158.

[7] G W. Mudd, S A. Svatek, L. Hague, O. Makarovsky, Z R. Kudrynskyi, C J. Mellor, Peter H. Beton , Laurence Eaves , Kostya S. Novoselov , Z D. Kovalyuk, E E. Vdovin, A J. Marsden, N R. Wilson, and A. Patanè, "High Broad-Band Photoresponsivity of Mechanically Formed InSe–Graphene van der Waals Heterostructures", Advanced. Materials, vol. 27, pp. 3760–3766, 2015. doi: 10.1002/adma.201500889.

[8] L-H. Zeng, M-Z. Wang, H. Hu, B. Nie, Y-Q. Yu, C-Y. Wu, L. Wang, J-G. Hu, C. Xie, F-X. Liang and L-B. Luo, "Monolayer Graphene/Germanium Schottky Junction As High-Performance Self-Driven Infrared Light Photodetector", ACS Appl. Mater. Interfaces, vol. 5, pp. 9362−9366. doi: 10.1021/am4026505.

[9] G. Faggio, A. Capasso, G. Messina, S. Santangelo, T. Dikonimos, S. Gagliardi, R. Giorgi, V. Morandi, L. Ortolani, N. Lisi, "High-temperature growth of graphene films on copper foils by ethanol chemical vapor deposition". J. Phys. Chem. C, vol. 117, pp. 21569, 2013.doi: 10.1021/jp407013y.

[10] S. Santangelo, G. Messina, A. Malara, N. Lisi, T. Dikonimos, A. Capasso, L. Ortolani, V. Morandi, G. Faggio, "Taguchi optimized synthesis of graphene films by copper catalyzed ethanol decomposition". Diam. Relat. Mater, vol. 41, pp. 73, 2014. doi: 10.1016/j.diamond.2013.11.006.

[11] C. Çelebi, C. Yanık, A G. Demirkol, İ. Kaya, "The effect of a SiC cap on the growth of epitaxial graphene on SiC in ultra high vacuum" Carbon, vo.50, pp.3026–31, 2012. doi: 10.1016/j.carbon.2012.02.088.

[12] H. Bencherif, L. Dehimi, F. Pezzimenti, F. G. Della Corte, "Temperature and SiO 2/4H-SiC interface trap effects on the electrical characteristics of low breakdown voltage

MOSFETs". Applied Physics A, vol.125(5), pp.294, 2019. doi: 10.1088/1674-4926/37/2/026001.

[13] M. Spera, D. Corso, S. Di Franco, G. Greco, A. Severino, P. Fiorenza, F. Roccaforte, "Effect of high temperature annealing (T> 1650° C) on the morphological and electrical properties of p-type implanted 4H-SiC layers", Materials Science in Semiconductor Processing, vol.93, pp.274-279, 2019. doi: 10.1016/j.mssp.2019.01.019.

[14] L.W. Ji, W. Water, Y.J. Hsiao, J.K. Tsai, K.T. Lam, T.H. Meen, Y.F. Chen, W.S. Shih, "TiO2-Based ultraviolet photodetectors", Integr. Ferroelectr. vol.143, pp.65–70, 2013. doi: 10.1080/10584587.2013.795848

[15] L. Laih, T. Chang, Y. Chen, W. Tsay, J. Hong, "Characteristics of MSM photodetectors with trench electrodes on P-type Si wafer", IEEE Trans. Electron Devices, vol.45, pp.2018–2023, 1998. doi: 10.1109/16.711369

[16] S.V. Averine, Y.C. Chan, Y.L. Lam, "Geometry optimization of interdigitated Schottky barrier metal–semiconductor–metal photodiode structures", Solid State Electron. Vol.45, pp.441–446, March 2002. doi: 10.1016/S0038-1101(01)00017-X

[17] H. Bencherif, F. Djeffal, H. Ferhati, "Performance enhancement of Pt/TiO2/Si UV-photodetector by optimizing light trapping capability and interdigitated electrodes geometry", Superlattices and Microstructures,vol.97, pp.303-312, 2016. doi: 10.1016/j.spmi.2016.06.028

[18] SZE, Simon M. et NG, Kwok K. Physics of semiconductor devices. John wiley & sons, 2006.

[19] C. Kenney, K. C. Saraswat, B. Taylor, P. Majhi, "Thermionic field emission explanation for nonlinear Richardson plots". IEEE Transactions on Electron Devices, vol.58(8), pp.2423-2429, 2011. doi: 10.1109/TED.2011.2156411

[20] H. Huang, Y. Xie, Z. Zhang, F. Zhang, Q. Xu, Z. Wu, H. Huang, Y. Xie, Z. Zhang, F. Zhang, Q. Xu, Z. Wu, "Growth and fabrication of sputtered TiO2 based ultraviolet detectors ", Appl. Surf. Sci. vol. 293, pp 248–254, 2014. doi: 10.1016/j.apsusc.2013.12.142

[21] Y. An, A. Behnam, E. Pop, A. Ural, "Metal-semiconductor-metal photodetectors based on graphene/p-type silicon Schottky junctions", Applied physics letters, vol.102(1), 013110, 2013. doi: 10.1063/1.4773992

[22] P. Ščajev, M. Kato, K. Jarašiūnas, "A diffraction-based technique for determination of interband absorption coefficients in bulk 3C-, 4H-and 6H-SiC crystals", Journal of Physics D: Applied Physics, vol.44(36), 365402, 2011. doi: 10.1088/0022-3727/44/36/365402

[23] A. Galeckas, P. Grivickas, V. Grivickas, V. Bikbajevas, J. Linnros, "Temperature dependence of absorption coefficient in 4H- and 6H-silicon carbide at 355 nm laser pumping wavelength", Phys. Status Solidi a, vol.191, pp.613–20, 2002. doi: 10.1002/1521-396X(200206)191:2-613.

[24] P. Grivickas, V. Grivickas, J. Linnros, A. Galeckas A, "Fundamental band edge absorption in nominally undoped and doped 4H-SiC", J. Appl. Phys. vol.101, 123521. doi: 10.1063/1.2749335.

[25] T. Stauber, N. Peres, N. M. R, A. K Geim, "Optical conductivity of graphene in the visible region of the spectrum". Physical Review B, vol.78(8), 085432, 2008. doi: 10.1103/PhysRevB.78.085432.

[26] L. A. Falkovsky, "Optical properties of graphene and IV–VI semiconductors", Physics-Uspekhi, vol.51(9), pp.887, 2008. doi:. 10.1070/PU2008v051n09ABEH006625.

[27] L. A. Falkovsky, "Optical properties of graphene", Journal of Physics: Conference Series vol. 129, pp. 012004, 2008. doi: 10.1088/1742-6596/129/1/012004.

[28] L. A. Falkovsky,A. A. Varlamov," Space-time dispersion of graphene conductivity", Eur.Phys.J.B, vol.56, pp. 281–284, 2007. doi: 10.1140/epjb/e2007-00142-3.
[29] M. L.Megherbi, F. Pezzimenti, L. Dehimi, M. A. Saadoune, F. G. Della Corte, "Analysis of Trapping Effects on the Forward Current–Voltage Characteristics of Al-Implanted 4H-SiC pin Diodes". IEEE Transactions on Electron Devices, vol. 65(8), pp. 3371-3378, 2018. doi: 10.1109/TED.2018.2849693.
[30] N. H. Rafat, "A simple analytical treatment of edge-illuminated VMJ silicon solar cells". Sol. Energy, vol.80, pp. 1588–1599, 2006. doi: 10.1016/j.solener.2005.12.004.
[31] R. F. Pierret, "Advanced Semiconductor Fundamentals", Prentice Hall/ Pearson Education, New Jersey, 2003.
[32] T. Trupke, M.A. Green, P. Wurfel, P.P. Altermatt, A.Wang, J. Zhao, et al., , "Temperature dependence of the radiative recombination coefficient of intrinsic crystalline silicon". J.Appl.Phys. vol. 94, pp. 4930–4937, 2003. doi: 10.1063/1.1610231.
[33] D.M. Caughey and R.E. Thomas, "Carrier mobilities in silicon empirically related to doping and field" Proc. IEEE, vol. 55, pp. 2192–2193, 1967. doi: 10.1109/PROC.1967.6123.
[34] S. Y. Davydov "On the electron affinity of silicon carbide polytypes". Semiconductors, vol. 41(6), pp. 696-698, 2007. doi: 10.1134/S1063782607060152.
[35] T. Kimoto and H. Matsunami, "High Quantum-Efficiency 4H-SiC UV Photodiode". Journal of the Korean Physical Society, vol. 30, No. 1, pp. 123-130, 1997. doi: 10.1109/LED.2010.2047239.
[36] A. Galeckas, , J. Linnros, V. Grivickas, U. Lindefelt, C Hallin, "Auger recombination in 4H-SiC: Unusual temperature behavior". Applied Physics Letters, vol. 71(22), pp. 3269-3271, 1997. doi: 10.1063/1.120309.
[37] A. Galeckas, J. Linnros, M. Frischholz, K. Rottner, N. Nordell, S. Karlsson, V. Grivickas, "Investigation of surface recombination and carrier lifetime in 4H/6H-SiC". Materials Science and Engineering: B, vol. 61, pp. 239-243, 1999. doi: 10.1016/S0921-5107(98)00510-8.
[38] Silvaco Atlas User's Manual, Device Simulator Software, 2013.
[39] H. Hodara, "Fiberoptic receiver performance: a tutorial review", Fibre integrated Opt, vol. 4(3), pp. 233-85, 1983. doi: 10.1080/01468038308205279.
[40] H. Matthews, "surface wave filters: design, construction, and use", New york : Wiley; 1977.
[41] W. C. Lien, D. S. Tsai, D. H. Lien, D. G. Senesky, J. H. He, A. P. Pisano, "4H–SiC Metal–Semiconductor–Metal Ultraviolet Photodetectors in Operation of 450K". IEEE Electron Device Letters, vol. 33(11), pp. 1586-1588, 2012. doi: 10.1109/LED.2012.2214759.
[42] J. Kim, W. B. Johnson, S. Kanakaraju, and K. S. Karim, "Improvement of dark current using InP/InGaAsP transition layer in large-area InGaAs MSM photodetectors," IEEE Trans. Electron Devices, vol. 51, no. 3, pp. 351–356, Mar. 2004. doi: 10.1109/TED.2003.822276.
[43] S. Potbhare, N. Goldsman, A. Lelis, J. M. Mcgarrity, F. B. Mclean, and D. Habersat, "A physical model of high temperature 4H–SiC MOSFETs," IEEE Trans. Electron Devices, vol. 55, no. 8, pp. 2029–2040, Aug. 2008. doi: 10.1109/TED.2008.926665.
[44] H. Bencherif, L. Dehimi, F. Pezzimenti, G. De Martino, F. G. Della Corte, "Multiobjective Optimization of Design of 4H-SiC Power MOSFETs for Specific Applications". Journal of Electronic Materials, vol. 48(6), pp. 3871-3880, 2019. doi: 10.1007/s11664-019-07142-5.

[45] F. Pezzimenti, H. Bencherif, A. Yousfi, L. Dehimi, “Current-voltage analytical model and multiobjective optimization of design of a short channel gate-all-around-junctionless MOSFET. Solid-State Electronics, vol. 161, pp. 107642. doi: 10.1016/j.sse.2019.107642.

[46] H. Bencherif, L. Dehimi, F. Pezzimenti, A. Yousfi, “Analytical model for the light trapping effect on ZnO: Al/c-Si/SiGe/c-Si solar cells with an optimized design”. In IEEE International Conference on Applied Smart Systems (ICASS) (pp. 1-6). 2018. doi: 10.1109/ICASS.2018.8651990.

[47] P. Vincent, D. S. Song, H. B. Kwon, D. K. Kim, J. H. Jung, J. H. Kwon, J. H. Bae, “Towards maximizing the haze effect of electrodes for high efficiency hybrid tandem solar cell”. Applied Surface Science, vol. 432, pp. 262-265, 2018. doi: 10.1016/j.apsusc.2017.07.204.

[48] P. Vincent, G. C. Sergio, J. Jang, I. M. Kang, P. Lang, H. Kim, J. H. Bae. ”Alternative approach to optimizing optical spacer layer thickness in solar cell using evolutionary algorithm”. In 2019 International Conference on Numerical Simulation of Optoelectronic Devices (NUSOD) (pp. 89-90). IEEE, 2019. doi: 10.1109/NUSOD.2019.8806865

[49] A. Selman, Z. Hassan, “Fabrication and characterization of metal–semiconductor–metal ultraviolet photodetector based on rutile TiO2 nanorod”, Mater. Res.Bull. vol. 73 , pp. 29–37, 2016. doi: 10.1016/j.materresbull.2015.08.013.